Semnan University

Journal of Heat and Mass Transfer Research

Journal homepage: http:// jhmtr.semnan.ac.ir

Forced Convective Heat Transfer of Non-Newtonian CMC-based CuO Nanofluid in a Tube

Morteza Bayareh*,[a], Nader Afshar [b]

[a] *Department of Mechanical Engineering, Shahrekord University, Shahrekord, Iran*
[b] *Esfahan Oil Refinery Company, Isfahan, Iran*

PAPER INFO

Paper history:
recieved: 2019-12-04
Revised: 2020-07-08
Accepted: 2020-07-08

Keywords:
Forced convective heat transfer;
Power-law
non-Newtonian nanofluid;
Reynolds number;
Nusselt number;
Constant heat flux.

ABSTRACT

In the present study, the thermal and rheological characteristics of power-law non-Newtonian CMC-based CuO nanofluid in a tube is studied using ANSYS FLUENT software. The tube is under a constant heat flux and nanofluid's viscosity is a function of shear rate and temperature. Two inlet velocity distributions of fully developed and uniform flow are employed. The volume fractions in the range of 0% to 4% and the Reynolds numbers in the range of 600 to 1500 are considered in the simulations. For both velocity profiles, the temperature and shear rate have considerable influences on the viscosity. Local heat transfer coefficient in the axial direction is enhanced by increasing the volume fraction. It was shown that the volume fractions less than 1.5% have an effect on local heat transfer slightly. It is revealed that as the Reynolds number increases, the local heat transfer and the average Nusselt number decrease. In conflict with the previous investigations, the present results show that the average Nusselt number is reduced by increasing the volume fraction of nanoparticles.

DOI: 10.22075/jhmtr.2020.19236.1262

1. Introduction

Nanofluids are suspensions of nanoparticles and have many applications in industries [1, 2]. The rheological and thermal characteristics of nanofluids have been considered by numerus investigators to provide some correlations between their properties. Several investigators have analyzed the natural and forced convection of nanofluids in enclosures experimentally and numerically [3-28].

Bayareh et al. [3] investigated Al_20_3-water nanofluid's effects on thermal characteristics of a c-shaped enclosure at the Reynolds number (Re) in the range of 10 to 1000. They found that as the Reynolds number and volume fraction of nanoparticles (φ) increase, the heat transfer is improved. The natural convective heat transfer in the wavy enclosures saturated with nanofluids was analyzed by Ahmed [6]. It was shown that as the waviness of enclosure surface increases, and the aspect ratio decreases, the Nusselt number enhances. Hojjat et al. [7] investigated the rheological characteristics of CuO- carboxymethyl cellulose (CMC), γ-Al_2O_3-CMC, and TiO_2-CMC nanofluids for the temperature in the range of 278 K to 318 K experimentally. Their results revealed that all nanofluids exhibit non-Newtonian shear thinning behavior.

Mariano et al. [9] studied the behavior of ethylene glycol-based SnO_2 nanofluid at the temperatures of 283.15 K, 303.15 K, and 323.15 K. Their observations showed the shear-thinning behavior of the nanofluid when the volume fraction of nanoparticles increases to 0.25.

The mixed convective heat transfer in a circular enclosure with a rotating inner cylinder was investigated by Shirazi et al. [11], and the mixed convection heat transfer in a square chamber with a rotating blade was studied by Sepyani et al. [12]. These investigations revealed that the rotation of inner circular cylinder or inner blade improves the heat transfer between enclosure walls and the fluid. Lahmar et al. [14] studied the effect of an inclined magnetic field on the thermal behavior of Fe_3O_4-water nanofluid flowing between two parallel plates. It was shown that the heat transfer is reduced by the presence of a magnetic field.

*Corresponding Author: Morteza Bayareh, Department of Mechanical Engineering, Shahrekord University, Shahrekord, Iran.
Email: m.bayareh@sku.ac.ir

Table 1. Main characteristics of convective heat transfer of nanofluids flowing in ducts, tubes, and enclosures.

Nanofluid	Newtonian/non-Newtonian	*Re*	*Pr*	*φ*	Ref.
Fe_3O_4–H_2O ferrofluids in an inclined partial open complex-wavy-walls ringed enclosures	Newtonian	†n/r	n/r	0-0.06	[2]
Al_20_3-water nanofluid in a c-shaped enclosure	Newtonian	10-1000	6.2	0-0.06	[3]
Buongiorno's nanofluid in a complex-wavy-wall surrounded enclosure	Newtonian	n/r	n/r	n/r	[5]
CuO-CMC, γ-Al_2O_3-CMC, and TiO_2-CMC nanofluids in a uniformly heated circular tube	Non-Newtonian	*Pe* = 210000-360000		0.001-0.015	[7]
Ethylene glycol-based SnO_2 nanofluid	Non-Newtonian	n/r	n/r	0-0.05	[9]
Carreau nanofluid flow over non-linearly stretched sheet	Non-Newtonian	n/r	2	n/r	[13]
Non-Newtonian nanofluids in three various microchannels	Non-Newtonian	*Pe* = 400 and 1385		0.01-0.04	[16]
Cu-water nanofluid flowing through a circular tube	Newtonian	*Pe* = 2500 and 6500		0.002-0.25	[20]
Al_2O_3-Xanthan non-Newtonian nanofluid flowing in a horizontal tube	Non-Newtonian	500-2500	n/r	0.01-0.06	[22]

†not reported

Esmaeilnejad et al. [16] used Al_2O_3 nanoparticles with a diameter of 30 nm suspended in the non-Newtonian base fluid. Nanofluid exhibited shear-thinning behavior and higher pressure drop as compared to the base fluid. Convective heat transfer of Al_2O_3-Xanthan non-Newtonian nanofluid flowing in a horizontal tube was investigated by Keshavarz Moraveji et al. [22] for the Reynolds number in the range of 500 to 2500. They proposed a correlation between Nusselt number, Reynolds number, Prandtl number, axial location, volume fraction, and viscosity of nanofluid and base fluid: Nu=2.14(Re D/x)^0.025 〖Pr〗^(1/3) φ^0.004 (μ_nf/μ_bf)^0.192.

Kamali and Binesh [25] employed MWCNT-based nanofluids to study the convective heat transfer in a tube with constant heat flux at Reynolds number in the range of 600 to 1200. They found that the Nusselt number of nanofluid is higher than that of base fluid for a given Reynolds number. As the Reynolds number increases, average Nusselt number is enhanced for both nanofluid and base fluid.

Table 1 summarizes the previous studies conducted on the thermal behavior of Newtonian and non-Newtonian nanofluids in ducts, tubes, and enclosures.

According to the previous experimental investigations, the shear viscosity is a strong function of temperature [26]. Conventional power-law relation does not consider the influences of temperature on the fluid viscosity. The main objective of the present study is that the viscosity is a function of shear rate and temperature. The high heat transfer capacity of non-Newtonian nanofluids makes them appropriate as coolant fluids for different systems such as microchannel and heat exchangers [16]. Forced convection heat transfer of power-law nanofluids flowing in a tube is investigated. The effects of φ and Re on heat transfer are discussed. Beside, a grid adaptation technique is employed in the present simulation.

2. Physics of Problem

According to the experimental study conducted by Garg et al. [10], who considered a circular tube with a diameter of 1.55 mm and a length of 914.4 mm, the tube is employed as a computational domain for the present simulations (Figure 1). The tube is under the constant heat flux of q^"=6000 W/m^2. Half of the tube is simulated due to its symmetry.

The boundary adaptation technique is employed to obtain high precision [29]. Grid adaptation method can be used for structured and unstructured grids using finite-element or finite-difference schemes. Adaptive meshing provides a very fine grid near the wall where the boundary layer must be captured. Sufficient grid points must exist in the boundary layer [30]. Figure 2 illustrates the schematic of the grid adaptation technique.

3. Governing equations and numerical method

Experimental observations demonstrated that when the cooling system is opened, it reaches the steady-state condition after 20 to 30 min [20]. Therefore, the unsteady effect can be neglected in the simulations. Based on the unsteady assumption, the governing equations are as follows [16]:

Continuity equation:

$$\nabla.\left(\rho_{nf}V\right)=0 \quad (1)$$

Momentum equation [16]:

$$\nabla.\left(\rho_{nf}VV\right)=-\nabla P+\nabla.\left(\eta_{nf}\nabla V\right) \quad (2)$$

Energy equation [16]:

$$\nabla.\left(\rho_{nf}Vc_{nf}T\right)=\nabla.\left(k_{nf}\nabla T\right) \quad (3)$$

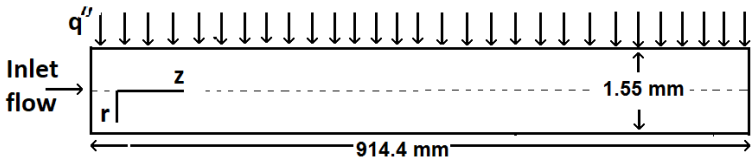

Figure 1. The schematic of the circular tube employed for the present simulations based on the experimental study conducted by Garg et al. [10].

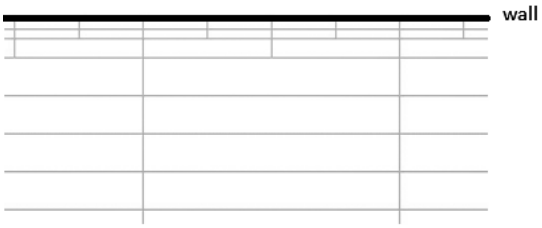

Figure 2. Adaptive meshing refining the cells close to the walls [29].

where $\boldsymbol{V}$ is the velocity vector, $\boldsymbol{\eta}$ is apparent viscosity, T is the temperature, and P the pressure. $\boldsymbol{\rho_{nf}}$, $\boldsymbol{c_{nf}}$, and $\boldsymbol{k_{nf}}$ are the density, specific heat capacity, and thermal conductivity of nanofluid, respectively.

$\boldsymbol{\eta_{nf}}$ and $\boldsymbol{k_{nf}}$ for the volume fractions of 0.5%, 1%, 1.5%, 3%, 4% are based on the data reported by Hojjat et al. [7] for the temperatures of 278 K, 288 K, 298 K, 308 K, and 318 K according to Eq. 4:

$$\eta_{nf} = \kappa \dot{\gamma}^{n-1} \tag{4}$$

where κ is the consistency index, $\dot{\gamma}$ is the shear rate, and n is the power-law index. Here, Eq. 5 is employed to calculate η_{nf}:

$$\eta_{nf} = C_1 \dot{\gamma}^{m-1}$$
$$C_1 = k_o exp\left[\alpha_{act}\left(\frac{1}{T} - \frac{1}{T_o}\right)\right] \tag{5}$$

where m is a new power-law index, C_1 is a new consistency index, α_{act} is the ratio of activation energy and thermodynamic constant, and T_o is a reference temperature. Table 2 presents the values of k_o, m, α_{act}, and T_o. In Figure 3, the variation of η_{nf} is plotted for φ= 4%. A comparison between the present results and the experimental data for φ = 4% is conducted in this figure. A good agreement between two results can be observed.

k_{nf} is:

$$k_{nf} = k_{bf}[0.981 + 0.00114T(°C) + 30.661\phi] \tag{6}$$

ρ_{nf} and C_{nf} are:

$$\rho_{nf} = \varphi\rho_p + (1-\varphi)\rho_{bf} \tag{7}$$
$$C_{nf} = \varphi C_p + (1-\varphi)C_{bf} \tag{8}$$

where subscripts *p* and *bf* are used for the nanoparticles and base fluid, respectively.

Since the Reynolds number varies from 600 to 1500, convection heat transfer of the nanofluid can be assumed to be laminar. Two inlet velocity profiles of hydrodynamically fully developed flow and uniform flow are employed. Thermal entrance length exists in the presence of an unheated starting length. The outflow condition is imposed on the outlet, i.e., all variables do not change at the tube outlet. An inlet temperature of 300 K is used for all simulations. Besides, the no-slip boundary condition is imposed on channel walls. The axisymmetric boundary condition is employed along the tube axial direction. A finite-difference approach is employed to solve the governing equations based on a single-phase fluid. Fluid is assumed to be a continuum phase. A SIMPLE algorithm is used for coupling the pressure and velocity fields. The PRESTO scheme is used to discretize the pressure and second-order upwind scheme is employed to discretize momentum and energy equations. Convergence is deemed acceptable when the continuity and momentum residuals decrease to the values of lower than 10^{-5}.

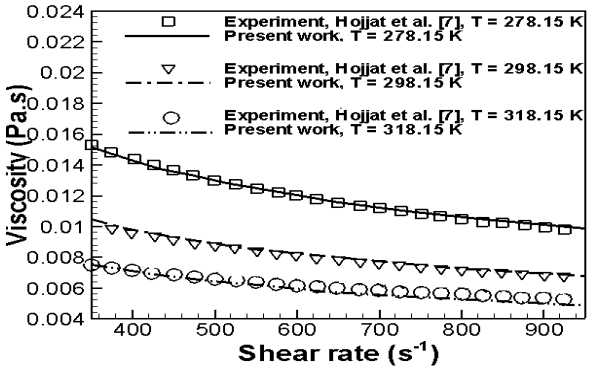

Figure 3. η_{nf} versus shear rate: comparison between the present results and the experimental data for φ = 4%.

Table 2. Values of k_o, m, , α_{act}, and T_o used in Eq. 5 for the volume fractions varied from 0% to 4% [7, 31].

Volume fraction (φ) %	m	k_o	α_{act}	T_o	R^2
0	0.5348	0.0782	1100.736	363.4572	0.997
0.5	0.5306	0.0126	1251.08	741.9133	0.998
1	0.538	0.0333	1120.375	487.541	0.998
1.5	0.5382	0.015	1645.9	494.9848	0.995
3	0.5641	0.0217	1453.774	459.8161	0.995
4	0.5681	0.0132	1543.877	534.9958	0.997

4. Results and discussion

In the present simulations, φ = 0% -4% and Re = 600-1500, leading to 48 case studies to investigate the laminar convection heat transfer of non-Newtonian nanofluids. Thus, only one case is selected in each section to describe the thermal and rheological characteristics of nanofluid.

4.1. Grid-independence test

Forced convection of the base fluid is simulated using four grid numbers of 41200, 82500, 155424, and 291250 at Re = 600. The values of Nu_{av} are shown in Figure 4 for different grid numbers. It is demonstrated that the grid numbers of 155424 and 291250 lead to relatively the same values for the average Nusselt number. Thus, the computational grid with 155424 nodes is selected for further simulations.

4.2. Verification

To validate the present simulations, Eq. 9 proposed by Siginer et al. [32] is employed for the case in which the fluid is hydrodynamically fully developed before heating.

$$Nu_z = 1.41\delta^{1/3}Gz^{1/3} \quad (9)$$

where

$$\delta = \frac{3m+1}{4m},\ Gz = Re\ Pr\frac{D}{z},\ Re = \frac{\rho_{nf}U^{2-m}D^m}{C_1},$$

$$Pr = \frac{C_{nf}\,C_1}{k_{nf}}\left(\frac{U}{D}\right)^{m-1}$$

U and *D* are the mean velocity of the fluid and tube diameter, respectively. Also, *Gz*, *Re*, and *Pr* are Graetz number, Reynolds number, and Prandtl number, respectively, and *z* refers to axial coordinate. It should be pointed out that the Prandtl number is changed from 3.5 to 24.

Siginer et al. [23] presented the following equation for a power-law fluid:

$$\frac{U_z}{U_{max}} = 1 - \left(\frac{2r}{D}\right)^{\frac{m+1}{m}} \quad (10)$$

where U_{max} refers to the maximum velocity. Figure 5 illustrates Nu_{av} for the case of base fluid obtained from the present simulations using $Nu_z = hD/k_{nf}$, where $h = q''/T_w - T_b$, and that obtained from Eq. 9 at the Reynolds number of 600. h is convection heat transfer coefficient, T_w is wall temperature and T_b is fluid bulk temperature. Figure 5 depicts that there is a good agreement between the results achieved by the simulations and Eq. 9 at Re = 600.

4.3. η_{nf} and k_{nf}

In the present simulations, $\eta_{nf} = f(\tau, T)$ and $k_{nf} = f(T)$ are considered. In this section, the variations of nanofluid viscosity and thermal conductivity along the tube are evaluated for φ = 3% and Re = 1200. It should be pointed out that the same results have been concluded for other values of φ and Re. Figure 6 compares the viscosity profile for two inlet conditions at three values of Z/D = 5, 25, and 100. This figure shows that the plots have the same trend when the inlet velocity has a fully development profile. It is obvious that as the temperature increases, the nanofluid viscosity decreases. For example, the viscosity is about 0.04 and 0.002 at r/R = 0 and 1, respectively, for z/D = 100. This is due to fact that the temperature is higher as the fluid becomes closer to the tube walls. In other words, in this case, the nanofluid viscosity at the tube center is 20 times that of at the tube surface. Besides, as the nanofluid moves along the tube, its viscosity enhances, especially in the tube's central region. For example, at r/R = 0.1, the viscosity of nanofluid is 0.028, 0.032, and 0.035 for z/D = 0, 25, and 100, respectively. This figure also shows the viscosity profile for the uniform flow distribution. It is observed that the trend of viscosity variation along the tube is completely different as r/R changes. This is due to fact that the fluid is not fully developed at the tube entrance. At z/D =100, the flow becomes fully developed and the viscosity variations are the same as those for fully developed flow. Figure 6 shows that the impact of constant heat flux on the uniform velocity profile increases with z/D. It is observed that the increase in the viscosity for the case of a uniform velocity profile is higher than that for the case of a fully developed velocity profile, especially at the central region of the tube. For example, at z/D = 100 and r/R = 0.1, nanofluid viscosity is 0.035 and 0.037 for fully developed and uniform velocity profiles, respectively.

Figure 7 shows the variation of nanofluid's k_{nf} versus r/R for different positions in the z-direction for φ = 3% at Re = 1200. For r/R < 0.5, the thermal conductivity remains

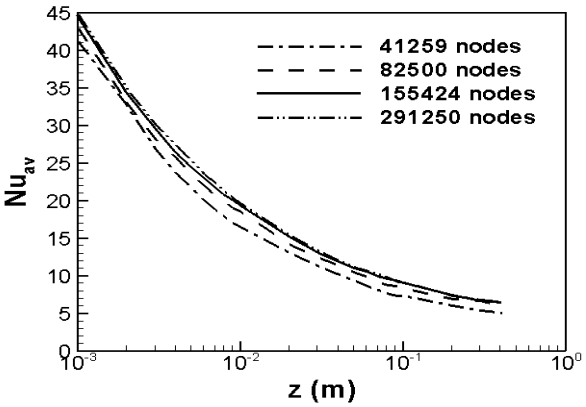

Figure 4. Average Nusselt number in the flow direction for different grid numbers.

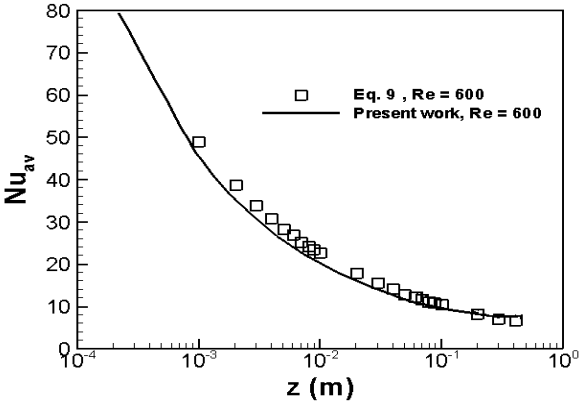

Figure 5. Nu_{av} versus z for the case of base fluid at Re = 600.

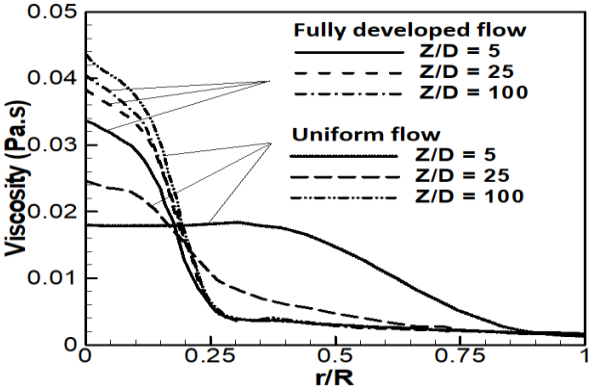

Figure 6. k_{nf} versus r/R for φ = 3% at Re = 1200.

constant along the tube. In other words, there is a central core in the tube in which the influence of heated walls is negligible. For r/R > 0.5, the thermal conductivity enhances with channel length. The figure demonstrates that higher temperature leads to larger k_{nf} for a constant z/D. For a given z/R, the thermal conductivity enhances along the radial direction from r/R = 0 to r/R = 1. This is due to fact that T_b increases along the axial and radial directions. This conclusion has been verified by Kamali and Binesh [25].

4.4. Forced convection heat transfer of non-Newtonian CMC-based CuO nanofluid

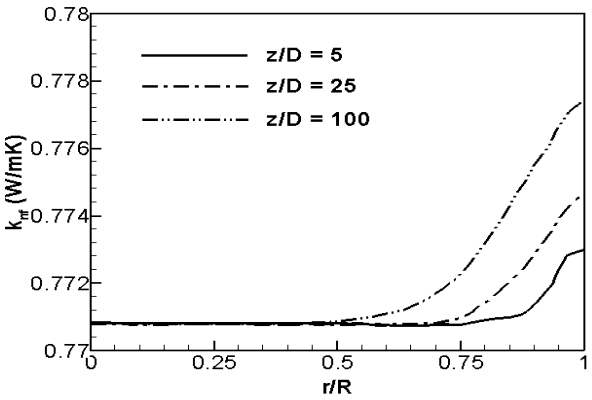

Figure 7. Thermal conductivity versus r/R at different positions in the z-direction for φ = 3% at Re = 1200.

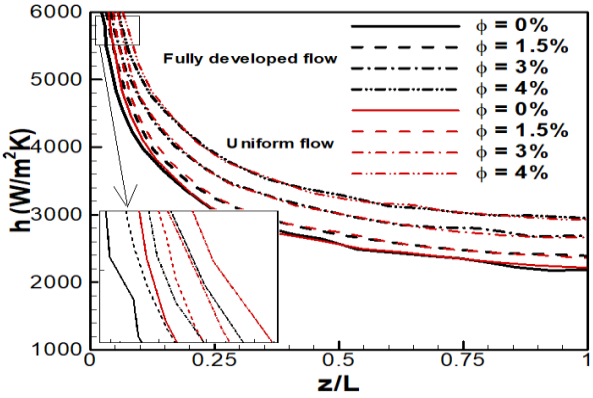

Figure 8. *h* for different values of φ at Re = 900.

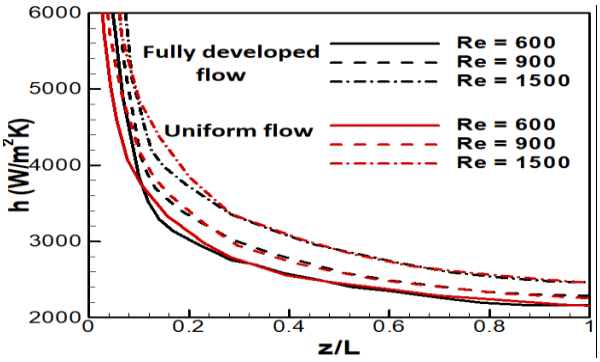

Figure 9. *h* versus z/L for φ = 1% and different values of Re.

In the present simulations, two inlet boundary conditions are used to evaluate the thermal and rheological characteristics of Cuo/CMC non-Newtonian nanofluid in a tube. Therefore, Re, φ, and inlet velocity distribution are crucial parameters. As mentioned previously, a case study is selected to describe the thermal characteristic of the nanofluid flow. In these simulations, Re = 900 and φ = 4% are considered. Figure. 8 illustrates the local convection heat transfer coefficient (*h*) for different volume fractions. It is shown that *h* of fully developed flow is slightly less than that of uniform flow.

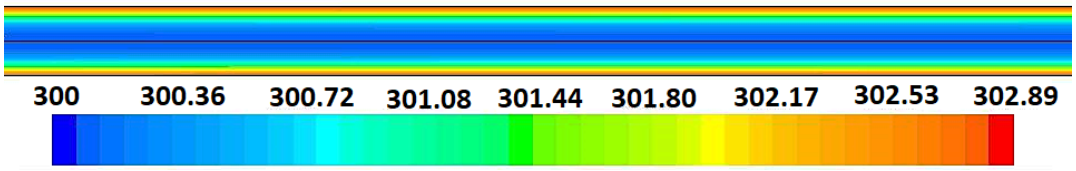

Figure 10. Temperature contours at φ = 4% and Re=1500 for uniform inlet velocity distribution.

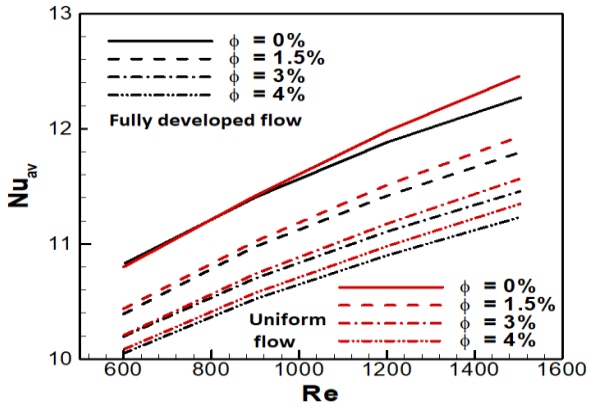

Figure 11. Nu_{av} for different values of Re and φ

For example, h = 5200 and 5045 W/m^{2}K for the uniform flow and fully developed velocity profiles, respectively at z/L = 0.1 and the volume fraction of 4%. This is due to a higher magnitude of the volume flow rate of uniform flow as compared to fully developed one. As mentioned before, uniform flow obtains a fully developed profile at z/D = 100. This means that the uniform flow has the same volume flow rate at this position. Figure 8 confirms that after the initial length of the tube, the heat transfer coefficient has identical values for both velocity profiles.

The effect of volume fraction can also be discussed using figure 8. Based on previous publications, as φ increases, h is enhanced [7, 8, 14-16]. The figure reveals that for a given value of z/L, h enhances with φ for both velocity profiles. For z/L < 0.15, the uniform flow and fully developed velocity profiles result in different values of h. However, for z/L > 0.15, the same magnitudes of h are achieved for both velocity profiles. As pointed out before, this is due to the fact that the uniform flow profile gets fully developed profile at this longitudinal section.

The effect of Re on h is illustrated in figure 9 for the volume fraction of 1%. It is concluded that the h increases with Re. As Re increases, the fluid flow becomes faster, resulting in an increase in the contact surface between fluid and hot walls. Thus, the distribution of heat becomes more uniform, and the bulk temperature of fluid increases. In other words, wall temperature is reduced, and the heat transfer rate is improved. This can be explained using Eq. 12; as the difference of $\bar{T}_w$ and $\bar{T}_b$ decreases, h increases. This conclusion is consistent with the previous investigations [22]. Figure 9 also compares the magnitude of h obtained along the tube using two different inlet velocity profiles. It is observed that the two profiles have the same trend, especially for a specific value of z/L. This value depends on the Reynolds number. As the Reynolds number increases, the uniform flow needs a longer length to reach a fully developed profile. For the range of Reynolds number studied in the present study, the convection heat transfer coefficient has the same value for different Reynolds numbers when z/L > 0.3.

It was found that the values of convection heat transfer are different for two inlet velocity conditions only for specific lengths of the tube, depending on φ and Re. Now, the Nu_{av} is calculated using Eq. 13 to evaluate the influences of Reynolds number and volume fraction of nanoparticles:

$$Nu_{av} = \frac{\bar{h}D}{k_{nf}} \tag{11}$$

$$\bar{h} = \frac{q''}{\bar{T}_w - \bar{T}_b} \tag{12}$$

where $\bar{T}_w$, $\bar{T}_b$, and $\bar{h}$ are average bulk temperature, wall temperature, and average heat transfer coefficient, respectively. It was found that k_{nf} of Cuo/CMC non-Newtonian nanofluid is a function of temperature. Since different temperature values are distributed along the tube, a constant value of k_{nf} for Cuo/CMC nanofluid cannot be determined. On the other hand, the temperature distribution for all cases is about 298±3 K. Hence, k_{nf} of nanofluids at 298 K is selected as a reference to calculate the average Nusselt number, i.e., $Nu_{av} = \bar{h}D/k_{nf}\big|_{298\,K}$. Figure 10 shows the temperature contours at φ = 4% and Re = 1500 for the uniform inlet velocity distribution.

Figure 11 illustrates Nu_{av} for different values of Re and φ for the fully developed and uniform velocity profiles. Contrary to previous investigations, present simulations demonstrate that Nu_{av} decreases by increasing φ. Nu is a function of Re number and Pr, i.e., Nu ~ Re^m Pr^n. Figure 11 reveals that as Re increases, Nu_{av} enhances. This is valid for two different inlet velocity profiles. At low Reynolds numbers, Nu_{av} calculated by uniform inlet velocity distribution is slightly higher than that obtained by using a fully developed velocity distribution. As Reynolds number increases, the difference between the Nusselt numbers of fully developed velocity and uniform velocity profiles becomes larger. For example, Nu_{av} = 10.38 and 10.44 are achieved for the fully developed velocity and uniform velocity profiles, respectively, at Re = 600 and volume fraction of 1.5%. The values of Nu_{av} are 11.79 and 11.93 for fully developed velocity and uniform velocity profiles, respectively, at Re = 1500 and φ = 1.5%. In other words, the value of Nu_{av} calculated for a fully

developed velocity distribution is 0.57% and 0.11% higher than that calculated for the uniform velocity profile when the Reynolds number increases from 600 to 1500.

Conclusion

The present paper investigated the thermal and rheological characteristics of power-law non-Newtonian CMC-based CuO nanofluid for φ = 0%-4%. The nanofluid's viscosity is a function of temperature and shear stress. Fully developed and uniform distributions were used for the inlet fluid flow. It was found that for r/R < 0.5, the thermal conductivity remains constant along the tube. In other words, there is a central core in the tube in which the influence of heated walls is negligible. For the range of Reynolds number studied in the present study, the convection heat transfer coefficient has the same value for different Reynolds numbers when z/L > 0.3. It was found that contrary to previous investigations, present simulations demonstrate that Nu_{av} decreases by increasing the volume fraction. As the Reynolds number increases, the difference between the values of Nu_{av} calculated for fully developed velocity profile and those obtained for uniform velocity profile increases.

Nomenclature

C Heat capacity
p Pressure (Pa)
q″ Heat flux (W/m^2)
Re Reynolds number
Pr Prandtl number
Gz Graetz number
T Temperature (K)
V Velocity vector (m/s)
k Consistency index
n Power-law index
K Thermal conductivity (W/m.K)
U Mean velocity (m/s)
T_0 Reference temperature (K)
C_1 New consistency index
D Tube diameter (1.55 mm)
R Tube radius (0.775 mm)
h Convectional heat transfer coefficient(W/m^2.K)
L Tube length (m)
Pe Peclet number

Greek symbols

μ Viscosity (Pa.s)
ρ Density (kg/m^3)
η Non-Newtonian viscosity (Pa.s)
$\dot{\gamma}$ Shear rate
ϕ Volume fraction
α_{act} Ratio of activation energy to thermodynamic constant
α Heat diffusion coefficient (m^2/s)

Subscripts

nf Nanofluid
bf Base fluid
p Nanoparticle
z Axial coordinate
r Radial coordinate
w Wall
b Bulk

References

[1] S. K. Das, S. U. S. Choi, W. Yu, T. Pradeep, Nanofluid: Science and Technology, John Wiley, New York, (2008).

[2] H. M. Elshehabey, Z. Raizah, H. F. Öztop, S. E. Ahmed, MHD natural convective flow of Fe_3O_4−H_2O ferrofluids in an inclined partial open complex-wavy-walls ringed enclosures using non-linear Boussinesq approximation, International Journal of Mechanical Sciences, 170, 105352 (2019).

[3] M. Bayareh, A. Kianfar, A. Kasaeipour, Mixed convection heat transfer of water-alumina nanofluid in an inclined and baffled c-shaped enclosure, Journal of Heat and Mass Transfer Research, 5(2), 129-138 (2018).

[4] M. Tajik Jamal-Abad, M. Dehghan, S. Saedodin, M. Valipour, A. Zamzamian, An experimental investigation of rheological characteristics of non- Newtonian nanofluids. Journal of Heat and Mass Transfer Research, 1(1), 17-23 (2014). doi: 10.22075/jhmtr.2014.150

[5] S. E. Ahmed, M. A. Mansour, A. M. Rashad, T. Salah, MHD natural convection from two heating modes in fined triangular enclosures filled with porous media using nanofluids, Journal of Thermal Analysis and Calorimetry, 2019. doi:10.1007/s10973-019-08675-x

[6] S. E. Ahmed, Effect of fractional derivatives on natural convection in a complex-wavy-wall surrounded enclosure filled with porous media using nanofluids, ZAMM - Journal of Applied Mathematics and Mechanics/Zeitschrift Für Angewandte Mathematik Und Mechanik, 2019. doi:10.1002/zamm.201800323

[7] M. Hojjat, S. Gh. Etemad, R. Bagheri, J. Thibault, Rheological characteristics of non-Newtonian nanofluids: Experimental investigation, International Communications in Heat and Mass Transfer, 38, 144–148 (2011).

[8] M. R. Eid, Effects of NP shapes on non-Newtonian bio-nanofluid flow in suction/blowing process with convective condition: Sisko model, Journal of Non-Equilibrium Thermodynamics, 2019. doi:10.1515/jnet-2019-0073

[9] A. Mariano, M. J. Pastoriza-Gallego, L. Lugo, A. Camacho, S. Canzonieri, M. M. Pineiro, Thermal conductivity, rheological behaviour and density of non-Newtonian ethylene

glycol-based SnO_2 nanofluids, Fluid Phase Equilibria, 337, , 119– 124 (2013).

[10] P. Garg, J. L. Alvarado, C. Marsh, T. K. Carlson, D. A. Kessler, K. Annamalai, An experimental study on the effect of ultrasonication on viscosity and heat transfer performance of multi-wall carbon nanotube-based aqueous nanofluids, International Journal of Heat and Mass Transfer, 52, 5090–5101 (2009).

[11] M. Shirazi, A. Shateri, M. Bayareh, Numerical investigation of mixed convection heat transfer of a nanofluid in a circular enclosure with a rotating inner cylinder, Journal of Thermal Analysis and Calorimetry, 133(2), 1061–1073 (2018).

[12] M. Sepyani, A. Shateri, M. Bayareh, Investigating the mixed convection heat transfer of a nanofluid in a square chamber with a rotating blade, Journal of Thermal Analysis and Calorimetry, 135, 609-623 (2019).

[13] M .R. Eid, K. L. Mahny, A. Dar, Muhammad T, Numerical study for Carreau nanofluid flow over a convectively heated nonlinear stretching surface with chemically reactive species, Physica A: Statistical Mechanics and Its Applications, 123063 (2019). doi:10.1016/j.physa.2019.123063

[14] S. Lahmar, M. Kezzar, M. R. Eid, M. R. Sari, Heat transfer of squeezing unsteady nanofluid flow under the effects of an inclined magnetic field and variable thermal conductivity, Physica A: Statistical Mechanics and Its Applications, 2019. doi:10.1016/j.physa.2019.123138 .

[15] M. N. Labib, M. J. Nine, H. Afrianto, H. Chung, H. Jeong, Numerical investigation on effect of base fluids and hybrid nanofluid in forced convective heat transfer, International Journal of Thermal Sciences, 71, 163-171 (2013).

[16] A. Esmaeilnejad, H. Aminfar, M. Shafiee Neistanak, Numerical investigation of forced convection heat transfer through microchannels with non-Newtonian nanofluids, International Journal of Thermal Sciences, 75, 76-86 (2014).

[17] N. Boumaiza, M. Kezzar, M. R. Eid, I. Tabet, On numerical and analytical solutions for mixed convection Falkner-Skan flow of nanofluids with variable thermal conductivity, Waves in Random and Complex Media, 1–20 (2019). doi:10.1080/17455030.2019.1686550.

[18] A. F. Al-Hossainy, M. R. Eid, M. Sh. Zoromba, SQLM for external yield stress effect on 3D MHD nanofluid flow in a porous medium, Physica Scripta 94(10), 105208 (2019).

[19] M. Tajik, M. Dehghan, A. Zamzamian, Analysis of variance of nanofluid heat transfer data for forced convection in horizontal spirally coiled tubes. Journal of Heat and Mass Transfer Research, 2(2), 45-50 (2015). doi: 10.22075/jhmtr.2015.348

[20] S. ZeinaliHeris, S. Gh. Etemad, M. Nasr Esfahany, Convective heat transfer of a Cu/Water nanofluid flowing through a circular tube, Journal of Experimental Heat Transfer, 32, 342-351 (2009).

[21] M. Sanaie-Moghadam, M. Jahangiri, F. Hormozi, Determination of stationary region boundary in multiple reference frames method in a mixing system agitated by Helical Ribbon Impeller using CFD. Journal of Heat and Mass Transfer Research, 2(1), 31-37 (2015). doi: 10.22075/jhmtr.2015.337

[22] M. Keshavarz Moraveji, S. M. H. Haddad, M. Darabi, Modeling of forced convective heat transfer of a non-Newtonian nanofluid in the horizontal tube under constant heat flux with computational fluid dynamics, International Communications in Heat and Mass Transfer, 39, 995–999 (2012).

[23] M. A. Ahmed, M. Z. Yusoff, N. H. Shuaib, Effects of geometrical parameters on the flow and heat transfer characteristics in trapezoidal-corrugated channel using nanofluid, International Communications in Heat and Mass Transfer, 42, 69–74 (2013).

[24] F. Bazdidi-Tehrani, S. M. Khanmohamadi, S. I. Vasefi, Evaluation of turbulent forced convection of non-Newtonian aqueous solution of CMC/CuO nanofluid in a tube with twisted tape inserts, Advanced Powder Technology, 31(3), 1100-113 (2020). doi:10.1016/j.apt.2019.12.022

[25] R. Kamali, A. R. Binesh, Numerical investigation of heat transfer enhancement using carbon nanotube-based non-Newtonian nanofluids, International Communications in Heat and Mass Transfer, 37, 1153–1157 (2010).

[26] H. S. Chen, Y. L. Ding, C. Q. Tan, Rheological behavior of nanofluids. New J Phys, 9, 1–25 (2007).

[27] S. Hussain, M. Jamal, S. E. Ahmed, Hydrodynamic forces and heat transfer of nanofluid forced convection flow around a rotating cylinder using finite element method: The impact of nanoparticles, International Communications in Heat and Mass Transfer, 108, 104310 (2019). doi:10.1016/j.icheatmasstransfer.2019.104310

[28] S. E. Ahmed, Z. Z. Rashed, MHD natural convection in a heat generating porous medium-filled wavy enclosures using

Buongiorno's nanofluid model, Case Studies in Thermal Engineering, 14, 100430 (2019).

[29] R. Ramakrishnan, Structured and unstructured grid adaptation schemes for numerical modeling of field problems. Applied Numerical Mathematics, 14(1-3), 285–310 (1994). doi:10.1016/0168-9274(94)90030-2

[30] M. Bayareh, S. Dabiri, A. M. Ardekani, Interaction between two drops ascending in a linearly stratified fluid, European Journal of Mechanics-B/Fluids, 60, 127-136 (2016). http://dx.doi.org/10.1016/j.euromechflu.2016.07.002

[31] A. Benchabane, K. Bekkour, Rheological properties of carboxymethyl cellulose (CMC) solutions. Colloid and Polymer Science, 286(10), 1173–1180 (2008). doi:10.1007/s00396-008-1882-2

[32] D. A. Siginer, D. D. Kee, R. P. Chhabra, Advances in flow and rheology of non-Newtonian fluids, 8th edition, Elsevier, Netherlands, (1999).